Optics Letters

Integrated programmable strongly coupled three-ring resonator photonic molecule with ultralow-power piezoelectric control

Jiawei Wang,[1] Kaikai Liu,[1] Andrei Isichenko,[1] Ryan Q. Rudy,[2] and Daniel J. Blumenthal[1,*]

[1]Department of Electrical and Computer Engineering, University of California Santa Barbara, Santa Barbara, California, USA
[2]DEVCOM Army Research Laboratory, Adelphi, Maryland 20783, USA
*danb@ucsb.edu

Received 1 December 2022; revised 30 March 2023; accepted 30 March 2023; posted 31 March 2023; published 26 April 2023

Photonic molecules can realize complex optical energy modes that simulate states of matter and have application to quantum, linear, and nonlinear optical systems. To achieve their full potential, it is critical to scale the photonic molecule energy state complexity and provide flexible, controllable, stable, high-resolution energy state engineering with low power tuning mechanisms. In this work, we demonstrate a controllable, silicon nitride integrated photonic molecule, with three high-quality factor ring resonators strongly coupled to each other and individually actuated using ultralow-power thin-film lead zirconate titanate (PZT) tuning. The resulting six tunable supermodes can be fully controlled, including their degeneracy, location, and degree of splitting, and the PZT actuator design yields narrow PM energy state linewidths below 58 MHz without degradation as the resonance shifts, with over an order of magnitude improvement in resonance splitting-to-width ratio of 58, and power consumption of 90 nW per actuator, with a 1-dB photonic molecule loss. The strongly coupled PZT-controlled resonator design provides a high-degree of resolution and controllability in accessing the supermodes. Given the low loss of the silicon nitride platform from the visible to infrared and the three individual bus, six-port design, these results open the door to novel device designs and a wide range of applications including tunable lasers, high-order suppression ultranarrow-linewidth lasers, dispersion engineering, optical parametric oscillators, physics simulations, and atomic and quantum photonics.

https://doi.org/10.1364/OL.482567

Photonic molecules (PMs) are systems of coupled atom-like optical resonators that produce rich quantized energy states and supermodes with behavior analogous to atoms and molecules [1]. These characteristics enable precision control of light and light–matter interactions including complex dispersion engineering [2] and nonlinear energy-level transitions [3], and applications including many-body physics simulations [4] and quantum optical phenomena [5]. The field of photonic molecules has evolved from the first demonstration of simple 2-coupled semiconductor optical cavities [6] to today's dual cavity, controllable, waveguide resonators capable of nonlinear 2-level transitions [3], symmetry breaking optical isolation [7], soliton optical frequency comb generation and dispersion engineering [8], and squeezed state sources [9]. Several PM energy state tuning mechanisms have been demonstrated including thermal [8,10], electro-optic [3], mechanical [11], optical [12], and acousto-optic [13]. However, to date, only electro-optic tuning has been shown to yield independent resonator tuning and low power dissipation [14]. The next stage of photonic molecule development requires scaling in terms of number of resonators per molecule, complexity of energy modes, controllability of the resonance linewidth and splitting, and low power dissipation actuation and fabrication in a wafer-scale CMOS foundry compatible photonic integration platform. Achieving these goals requires a fully planar fabrication process of low-loss waveguides and high-quality factor (Q) coupled resonators that can be independently tuned with low-power actuation that maintains the low loss and high Q. Advances in photonic molecule scaling, control, and integration will enable new applications including tunable lasers, dispersion engineering, nonlinear frequency synthesis, analog optical computation and quantum photonic circuits, and physics simulations.

Progress in photonic molecule integration has been limited to coupling between a single bus to two- and three-coupled microring resonators [15,16], microdisks [17], and photonic crystals [18]. More recent dual resonator advances include electro-optically tunable molecules for soliton optical frequency comb generation [8] and an optical isolator without tuning [7]. These demonstrations have had limited tunability, symmetry, and bus coupling, where molecules with more than two resonators are limited to chain-linked two–two coupling [19] or serially coupling [11]. Additionally, thermal tuning for DC bias control has limited power scalability and low linewidth resolution due to low Q and high loss [15]. For more complex coupled resonator circuits, it is critical to enable DC bias resonance tuning of each resonator independently using low-power actuators. In addition to DC tuning and biasing, it is also desirable to use actuators that can be modulated in the MHz to GHz range. Low-power PZT stress-optic actuators are able to maintain low optical waveguide losses and high optical Q with static (DC) tuning capabilities as

well as AC modulation, and offer low cross talk [20]. Other stress-optic modulation approaches include resonant AC aluminum nitride (AlN) modulators [21]. The choice of stress-optic actuator should be compatible with fully planar, ultralow-loss platforms, without requiring complex under-etching processes [22] and maintain low optical losses across the visible to IR.

In this paper, we report demonstration of a photonic molecule (PM) composed of three fully coupled all-waveguide silicon nitride high-Q, PZT tunable ring resonators, with each resonator strongly coupled to each other and its own independent waveguide. Static tuning and narrow linewidth modes are realized using monolithically integrated, ultralow-power dissipation PZT actuators [20] that are compatible with the silicon nitride platform [23] and maintain the high resonator Q. The PM is composed of three coupled 580-μm radius silicon nitride ring resonators, with a measured 43-MHz full width at half maximum (FWHM) resonance width and a 48-GHz free spectral range (FSR). An intrinsic Q of 8.11 million is measured at 1550 nm for the single resonator that has the same geometry and waveguide design of the three resonators in the PM, the highest reported Q to date for a PZT controlled silicon nitride waveguide resonator. The high-resolution supermode splitting is due to the strong coupling between the high-Q resonators, and can be tuned by 2.5 GHz with a 0–15-V DC applied voltage while maintaining the narrow linewidth below 58 MHz across the full tuning range with a tuning sensitivity of 160 MHz/V and low power consumption of 90 nW per actuator. A large mode splitting to linewidth ratio of 58 is achieved, which is over an order of magnitude increase compared to a similar integrated thermally tunable six supermode 3-ring PM structure [15] of 2.8. We use a coupled mode theory (CMT) matrix model to accurately simulate and predict the resonance tuning and splitting, showing excellent agreement with experimental measurements. Our model provides a robust tool for photonic molecule device design and enables control of photonic molecules for integrated photonic applications including photonic molecule combs [8] and photonic molecule quantum photonics [5].

The photonic molecule is shown in Fig. 1(a) with the three coupled ring–bus resonators symmetric to the three-axes angled at 120-degrees offset as indicated by the dotted lines. The waveguide and actuator structures are fully planar monolithic as shown in Fig. 1(b) (see Supplement 1 for details on fabrication) without requiring undercut or released tuning structures and

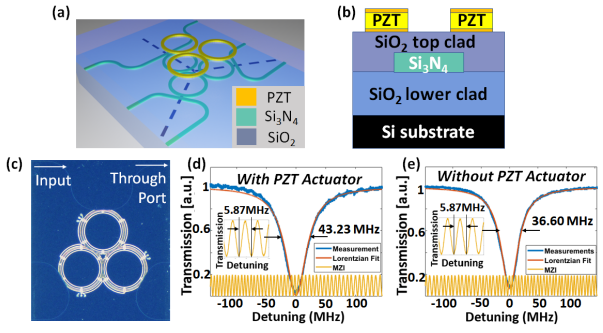

Fig. 1. (a) 3D illustration of the PZT controlled photonic molecule. (b) PZT controlled waveguide cross section geometry. (c) Optical micrograph of a fabricated device with monolithically integrated lead zirconate titanate (PZT) actuators. (d) and (e) Quality factor (Q) measurement of a single-ring resonator with R = 580 μm with and without the PZT actuator.

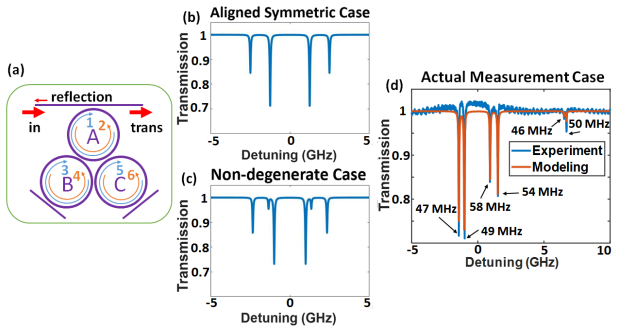

Fig. 2. (a) Illustration of the three-coupled-resonator system, where each photonic atom has two split states because of the clockwise and counterclockwise propagating fields due to mutual coupling. (b) Simulated transmission spectrum of the aligned degenerate case with identical resonators and coupling coefficients. (c) Non-degenerate case occurring when the coupling strength between the photonic atoms are unbalanced, and symmetry is broken. (d) Measured and modeled PM transmission spectra for a single bus.

waveguides. The individual resonator design is a 580-μm radius with 1.5-μm ring–bus coupling gap and the waveguide geometry is 175 nm thickness and 2.2 μm wide. The PZT actuator is designed with a 2-μm horizontal offset gap from the waveguide center to avoid overlap with the optical mode and maintain low optical loss and high Q while realizing a large strain-optic effect and index and resonance shift [20]. The optical microscopy image of the fabricated device is shown in Fig. 1(c).

We measure the resonance FWHM of the single-ring resonator to be 43.23 MHz at 1550 nm, as shown in Fig. 1(d), using a radio frequency calibrated unbalanced Mach–Zehnder interferometer (MZI) [24]. These measurements correspond to an intrinsic Q of 8.11 million and loaded Q of 4.48 million, corresponding to a propagation loss of 3.3 dB/m. As a comparison, the resonator of the same geometry but without the PZT actuator has a resonance FWHM of 36.60 MHz, as shown in Fig. 1(e), corresponding to an intrinsic Q of 8.37 million and propagation loss of 3.19 dB/m. The loss is increased by only 3%, demonstrating that the monolithically integrated PZT actuators maintain the properties of the ultralow-waveguide loss and high Q. The photonic molecule insertion loss is estimated to be 1 dB from the through port, with a coupling loss measured with a straight waveguide to be 5 dB from double sides.

A CMT model [25] is used to simulate and predict the supermode behavior, validate the resonance and splitting structure, and enable programming of desired spectral properties. We employ a matrix approach to model the fully coupled three-ring photonic molecules that includes the waveguide loss, bus–ring and ring–ring coupling coefficients, and effective mode index (see Supplement 1 for details on modeling). Models for three-resonator photonic molecules have also been described in [16].

Each resonator supports two modes [shown in Fig. 2(a)], defining the clockwise (CW) and the counterclockwise (CCW) coupled propagating fields, and six supermodes are supported due to the strong coupling between all three resonators (see Supplement 1). Mode splitting due to backscattering in each resonator, such as particles, defects, or sidewall roughness, is not observed as in [24] due to the larger linewidth compared to scattering induced splitting in this resonator design. Each photonic atom (resonator) can be considered to have two split states with

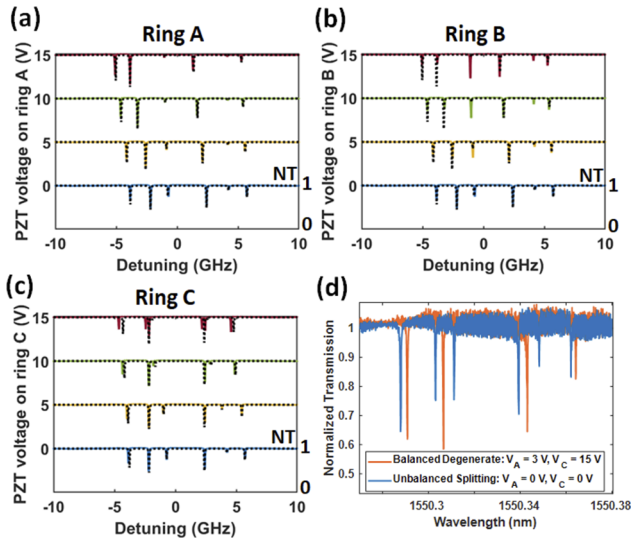

Fig. 3. (a)–(c) DC biasing of rings A, B, and C. The colored lines indicate the measured transmission spectrums as DC bias is adjusted from 0 to 15 V, and the dashed black lines are the coupled photonic molecule model fitting. (d) Symmetric case reached by tuning multiple rings. N.T., normalized transmission.

Table 1. Comparison with Prior Three-Resonator PM Works[a]

Ref.	This Work	[15]	[19]	[11]
Configuration	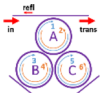	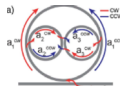	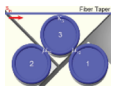	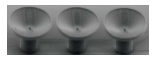
Integration	Yes	Yes	No	No
Material	Si_3N_4 / SiO_2	SOI	Silica toroid	Polymeric Silicone
Tunability	PZT	Microheater	Temperature control (TEC)	Mechanical Stretching
Loaded Q	4.48 M	6.7 K	29, 37, and 110 M	79 K
Linewidth	43 MHz	29 GHz *	6.8–1.8 MHz	NA
Supermodes	6	6	3	NA
Detuning Range	2.5 GHz	80 GHz	0.75 GHz *	NA
Resonance Splitting to Linewidth Ratio	58	2.8	110	NA
Power Consumption	90 nW per actuator	35 mW	NA	NA
Drop ports	4	0	0	0

[a]SOI, silicon on insulator; TEC, thermoelectric cooler. The asterisk denotes extracted based on the information provided in the literature.

a bonding orbital and an antibonding orbital as in the hydrogen molecule model, where these states coherently add to generate supermodes. We study three mode-splitting cases as depicted in Figs. 2(b)–2(d). When all resonators and waveguides and coupling parameters are identical, the energy modes are degenerate with four supermodes, as shown in the transmission spectrum in Fig. 2(b), the rightmost supermode as the highest energy level and the leftmost supermode the lowest energy level. The four remaining supermodes are present in two degenerate pairs [26]. When symmetry is broken, for example, if the coupling strengths κ between the resonators are non-uniform, the middle degenerate pairs split and mode degeneracy is lifted [Fig. 2(c)]. The measured transmission spectrum for input to output for one of the resonators is shown in Fig. 2(d) and busses for the other two resonators serve as add/drop ports (see Supplement 1). Fabrication variations among resonators and coupling lead to asymmetric molecule energy, as shown in the experimental and modeled energy spectra in Fig. 2(d), and the six supermodes have well-defined resonances with narrow linewidths of 47 MHz, 49 MHz, 58 MHz, 54 MHz, 46 MHz and 50 MHz, and corresponding loaded Q of 4.12 million, 3.95 million, 3.34 million, 3.58 million, 4.21 million, and 3.87 million, respectively. The measured spectrum (blue) is in good agreement with the CMT matrix model fitting (orange) that incorporates measured cavity loss γ and inter-ring coupling coefficients κ. This model allows us to accurately design and predict the mode energy splitting, which becomes increasingly important as the energy state complexity of photonic molecules increases and to enable calibration due to fabrication and environmental perturbations.

We demonstrate PM supermode tuning by controlling the PZT DC bias for each ring resonator. Independent DC bias for each ring resonator enables full control over supermode splitting and frequency location. An example is shown in Figs. 3(a)–3(c).

The colored lines indicate the measured transmission spectra as the DC bias voltages applied to the PZT actuators are adjusted from 0 V to 15 V on each ring. The modeled behavior, given by the dashed lines, are in strong agreement with the measurements, yielding an important tool for designing, predicting, and accurately controlling the supermodes. By tuning two of the resonators at the same time, the symmetric degenerate case can be reached, as shown in Fig. 3(d), demonstrating that we can calibrate and balance the photonic molecule as well as tune the energy splitting. The PZT material has high resistivity resulting in a very low leakage current and power dissipation, measured to be approximately 6 nA at 15-V bias, corresponding to 90-nW electrical power consumption per actuator. The capacitance of the PZT actuator is measured to be approximately 600 pF, corresponding to a stored energy of 67 nJ at 15 V.

In conclusion, we have demonstrated a monolithically integrated, programmable strongly coupled three-ring resonator photonic molecule. The molecule consists of silicon nitride three-ring resonators with intrinsic Q of 8.11×10^6, the highest reported to date for a PZT controlled integrated ring resonator. The ability to maintain high Q via PZT actuation without degradation as the resonance shifts results in narrow PM resonance linewidths that are independent of the tuning and state splitting, and a resonance splitting to a linewidth ratio of 58, representing the lowest linewidth for a PZT tunable resonator and over an order of magnitude improvement in resonance split to linewidth ratio for a prior integrated three-resonator PM [15]. The PZT actuator offers 90-nW ultralow-power dissipation with a linear tuning coefficient of 160 MHz/V. The devices are fabricated with a CMOS foundry compatible process without requiring complex processes like under-cut or released and suspended structures.

A comparison of the performance for this work to other three-coupled resonator photonic molecules is given in Table 1.

The PZT actuation provides a programmable PM platform that increases the design and spectral flexibility and the potential to scale to larger arrays due to lower power and compact size. The multiple discrete levels of the photonic molecule can be utilized as a signal splitter or a wavelength shifter with proper PZT spatiotemporal modulation [20] and can enable new integrated circuits for tunable dispersion compensators [8], optical frequency comb generation [27], and optical parametric oscillation by tuning the phase-matched modes [28]. These results provide

a path toward integration of photonic molecules for applications like multichannel high-order filters [16], topological photonics [2], ultralow phase noise lasers through higher-order mode inhibition of stimulated Brillouin lasers (SBL) through mode splitting [29], and many-body physics simulations [4]. The low power consumption is critical to enable large-scale integration of coupled photonic atoms and complex photonic molecules on a chip, and suited for heterogeneous integration with semiconductor lasers.

Funding. National Science Foundation (1745612); DEVCOM Army Research Laboratory (W911NF-22-2-0056).

Acknowledgments. The authors would like to thank Steven Isaacson of General Technical Services for his efforts in fabrication. A.I. acknowledges the support from the National Defense Science and Engineering Graduate (NDSEG) Fellowship Program.

Disclosures. The authors declare no conflicts of interest.

Data availability. Data underlying the results presented in this paper are not publicly available at this time but may be obtained from the authors upon reasonable request.

Supplemental document. See Supplement 1 for supporting content.

REFERENCES

1. S. V. Boriskina, in *Photonic Microresonator Research and Applications*, I. Chremmos, O. Schwelb, and N. Uzunoglu, eds., Springer Series in Optical Sciences (Springer US, 2010), pp. 393–421.
2. L. Lu, J. D. Joannopoulos, and M. Soljačić, Nat. Photonics **8**, 821 (2014).
3. M. Zhang, C. Wang, Y. Hu, A. Shams-Ansari, T. Ren, S. Fan, and M. Lončar, Nat. Photonics **13**, 36 (2019).
4. M. J. Hartmann, F. G. S. L. Brandão, and M. B. Plenio, Laser Photonics Rev. **2**, 527 (2008).
5. K. Liao, X. Hu, T. Gan, Q. Liu, Z. Wu, C. Fan, X. Feng, C. Lu, Y. Liu, and Q. Gong, Adv. Opt. Photonics **12**, 60 (2020).
6. M. Bayer, T. Gutbrod, J. P. Reithmaier, A. Forchel, T. L. Reinecke, P. A. Knipp, A. A. Dremin, and V. D. Kulakovskii, Phys. Rev. Lett. **81**, 2582 (1998).
7. L. Chang, X. Jiang, S. Hua, C. Yang, J. Wen, L. Jiang, G. Li, G. Wang, and M. Xiao, Nat. Photonics **8**, 524 (2014).
8. Ó. B. Helgason, F. R. Arteaga-Sierra, Z. Ye, K. Twayana, P. A. Andrekson, M. Karlsson, J. Schröder, and Victor Torres-Company, Nat. Photonics **15**, 305 (2021).
9. Y. Zhang, M. Menotti, K. Tan, V. D. Vaidya, D. H. Mahler, L. G. Helt, L. Zatti, M. Liscidini, B. Morrison, and Z. Vernon, Nat. Commun. **12**, 2233 (2021).
10. S. Woska, P. Rietz, O. Karayel, and H. Kalt, Opt. Mater. Express **11**, 3194 (2021).
11. T. Siegle, S. Schierle, S. Kraemmer, B. Richter, S. F. Wondimu, P. Schuch, C. Koos, and H. Kalt, Light: Sci. Appl. **6**, e16224 (2017).
12. Y. Sato, Y. Tanaka, J. Upham, Y. Takahashi, T. Asano, and S. Noda, Nat. Photonics **6**, 56 (2012).
13. S. Kapfinger, T. Reichert, S. Lichtmannecker, K. Müller, J. J. Finley, A. Wixforth, M. Kaniber, and H. J. Krenner, Nat. Commun. **6**, 8540 (2015).
14. M. Li, J. Ling, Y. He, U. A. Javid, S. Xue, and Q. Lin, Nat. Commun. **11**, 4123 (2020).
15. M. C. M. M. Souza, G. F. M. Rezende, L. A. M. Barea, A. A. G. von Zuben, G. S. Wiederhecker, and N. C. Frateschi, Opt. Lett. **40**, 3332 (2015).
16. M. A. Popovíc, T. Barwicz, M. R. Watts, P. T. Rakich, L. Socci, E. P. Ippen, F. X. Kärtner, and H. I. Smith, Opt. Lett. **31**, 2571 (2006).
17. E. Gil-Santos, C. Baker, A. Lemaitre, C. Gomez, S. Ducci, G. Leo, and I. Favero, Nat. Commun. **8**, 14267 (2017).
18. C. Jarlov, K. A. Atlasov, L. Ferrier, M. Calic, P. Gallo, A. Rudra, B. Dwir, and E. Kapon, Opt. Express **21**, 31082 (2013).
19. C. Yang, X. Jiang, Q. Hua, S. Hua, Y. Chen, J. Ma, and M. Xiao, Laser Photonics Rev. **11**, 1600178 (2017).
20. J. Wang, K. Liu, M. W. Harrington, R. Q. Rudy, and D. J. Blumenthal, Opt. Express **30**, 31816 (2022).
21. J. Liu, H. Tian, E. Lucas, A. S. Raja, G. Lihachev, R. N. Wang, J. He, T. Liu, M. H. Anderson, W. Weng, S. A. Bhave, and T. J. Kippenberg, Nature **583**, 385 (2020).
22. W. Jin, R. G. Polcawich, P. A. Morton, and J. E. Bowers, Opt. Express **26**, 3174 (2018).
23. D. J. Blumenthal, R. G. Heideman, D. Geuzebroek, A. Leinse, and C. Roeloffzen, Proc. IEEE **106**, 2209 (2018).
24. M. W. Puckett, K. Liu, N. Chauhan, Q. Zhao, N. Jin, H. Cheng, J. Wu, R. O. Behunin, P. T. Rakich, K. D. Nelson, and D. J. Blumenthal, Nat. Commun. **12**, 934 (2021).
25. M. C. M. M. Souza, G. F. M. Rezende, L. A. M. Barea, G. S. Wiederhecker, and N. C. Frateschi, Opt. Express **24**, 18960 (2016).
26. E. F. Franchimon, K. R. Hiremath, R. Stoffer, and M. Hammer, J. Opt. Soc. Am. B **30**, 1048 (2013).
27. Ó. B. Helgason, M. Girardi, Z. Ye, F. Lei, J. Schröder, and V. T. Company, "Power-efficient soliton microcombs," arXiv, arXiv:2202.09410 (2022).
28. J. A. Black, G. Brodnik, G. Brodnik, H. Liu, H. Liu, S.-P. Yu, S.-P. Yu, D. R. Carlson, D. R. Carlson, J. Zang, J. Zang, T. C. Briles, S. B. Papp, and S. B. Papp, Optica **9**, 1183 (2022).
29. K. Liu, M. W. Harrington, K. D. Nelson, R. O. Behunin, S. B. Papp, and D. J. Blumenthal, in *Conference on Lasers and Electro-Optics* (Optica Publishing Group, 2022), p. SF2K.1.